Structural transitions in a NiTi alloy:
a multistage loading-unload cycle

V. Di Cocco

University of Cassino, DiMSAT, via G. Di Biasio 43, 03043, Cassino (FR), Italy.
v.dicocco@unicas.it

C. Maletta

University of Calabria, Dip. of Mechanical Engineering, 87036 Rende (CS), Italy.
carmine.maletta@unical.it

S. Natali

University of Rome "Sapienza", D.I.C.M.A., via Eudossiana 18, 00185 Roma, Italy.
stefano.natali@uniroma1.it

ABSTRACT. NiTi shape memory alloys (SMAs) are increasingly used in many engineering and medical applications, because they combine special functional properties, such as shape memory effect and pseudo-elasticity, with good mechanical strength and biocompatibility. However, the microstructural changes associated with these functional properties are not yet completely known. In this work a NiTi pseudo-elastic alloy was investigated by means of X-ray diffraction in order to assess micro-structural transformations under mechanical uniaxial deformation. The structure after complete shape recovery have been compared with initial state.

SOMMARIO. Le leghe a memoria di forma costituite da nickel e da titanio sono sempre più utilizzate in molti settori dell'ingegneria e della medicina, in quanto combinano speciali proprietà funzionali, quali la memoria di forma e la pseudo-elasticità, con buone caratteristiche meccaniche e di biocompatibilità. Tuttavia, le trasformazioni mico-strutturali che conferiscono tali proprietà funzionali non sono ancora completamente note. In questo lavoro è stata analizzata una lega NiTi pseudo-elastica, mediante indagini diffrattometriche ai raggi X, al fine di mettere in evidenza le modificazioni strutturali che intervengono sotto l'effetto di deformazioni imposte. La microstruttura ottenuta dal completo recupero della forma è stata confrontata con quella iniziale.

KEYWORDS. Shape Memory alloys; Stress-induced martensitic transformation; X-Ray analyses.

INTRODUCTION

Shape memory alloys (SMAs) are an important class of metallic alloy which exhibit unique features with respect to common engineering alloys, such as the shape memory effect (SME) and pseudo-elastic effect (PE). In particular, due to these properties SMAs are able to recover their original shape after high values of mechanical deformations, by heating up to a characteristic temperature (SME) or simply by removing the mechanical load (PE). Different kinds of shape memory alloys have been exploited in the last decades, such as the copper-zinc-aluminum (ZnCuAl), copper-aluminum-nickel (CuAlNi), nickel-manganese-gallium (NiMnGa), nickel-titanium (NiTi), and other SMAs created by

alloying zinc, copper, gold, iron, etc. Within this class of materials the near equiatomic NiTi binary system shows the most exploitable characteristics and it is currently used in an increasing number of applications in many fields of engineering [1], for the realization of smart sensors and actuators, joining devices, hydraulic and pneumatic valves, release/separation systems, consumer applications and commercial gadgets. However, due to their good biocompatibility the most important applications of NiTi alloys are in the field of medicine, where the pseudo-elasticity is mainly exploited for the realization of several components such as cardiovascular stent, embolic protection filters, orthopedic components, orthodontic wires, micro surgical and endoscopic devices.

From the microstructural point of view shape memory and pseudo-elastic effects are due to a reversible solid state microstructural transitions from austenite to martensite, which can be activated by mechanical and/or thermal loads [2].

The phase transition of near equiatomic NiTi systems is illustrated in the phase diagram of Fig. 1, where at T<900°C complete temperature transformations are not well specified. In the last years a triple transitions has been accepted, from an austenitic B2 phase for slowly cooling a B19 orthorhomic phase transformation occurs, but for long time at 500°C (about 120 hours) an monoclinic B19' phase is obtained. But not all the transformation are possible when changing the Ni content; in particular when increasing the Ni content last transformation (B19') can take place only under environmental temperature or under the zero absolute [3-11].
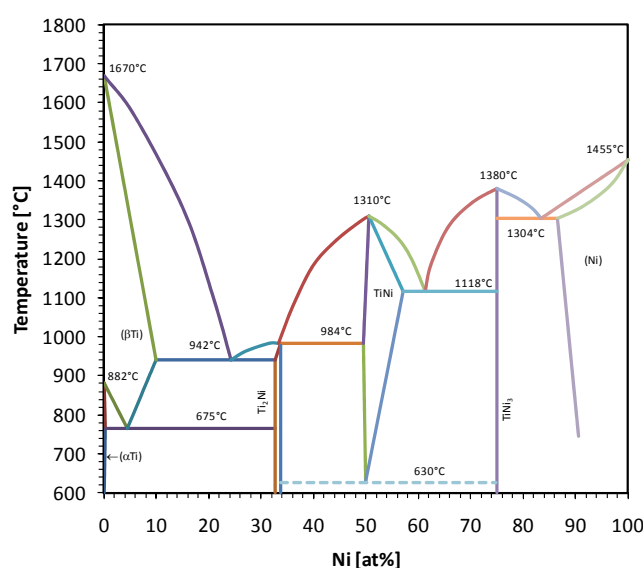

Figure 1: NiTi alloy phase diagram.

The near equiatomic NiTi system is capable of two successive martensitic phase transformations during cooling from its high temperature austenitic phase. In Ti rich NiTi SMAs, the first phase transformation during cooling is observed just above room temperature and results in the R-phase, the second one occurs around room temperature and results in M-phase (monoclinic structure), often with a fine lath morphology. These transformations give rise to thermo-elasticity and twin deformations in NiTi alloy facilitating shape memory effect (SME) [12-14].

Elastic strain energy provides the reversible nonchemical contribution to the overall free energy of the system. The method of elastic strain energy generation depends upon whether or not external stress is applied. In the absence of external stress, the martensite transformations in NiTi produce a self-accommodating arrangement of martensite correspondent variant pairs (CVPs) that minimizes elastic strain energy. As the volume fraction of self-accommodating groups (SAGs) of martensite CVPs grows, the concomitant increases in interfacial energy and elastic strain raise the stored elastic strain energy of the system. The evolution of microstructure and the formation of microcracks during cyclic loading has been observed and crack propagation under cyclic loading conditions has been monitored in many works, but behavior of cracks under static loading conditions in martensitic, pseudo-plastic and austenitic pseudo-elastic NiTi microstructures is not yet clear [8, 15-19].

In this work the mechanical properties of a commercial NiTi shape memory alloy have been investigated by tensile tests of miniaturized dog bone shaped specimens carried out by using a mini testing machine. In addition, *in situ* XRD analyses were performed during mechanical tests, in order to understand the influence of microstructure and crystallographic parameter on the pseudo-elastic effect of the alloy, as well as on the related hysteresis in the stress-strain response.

MATERIAL AND METHODS

In this work a commercial pseudo-elastic NiTi alloy (Type S, Memory metalle, Germany), with nominal chemical composition of 50.8at.% Ni - 49.2 at.% Ti, was used to investigate the evolution of microstructure during loading-unloading cycle. In Fig. 2 light micrographs of the initial austenitic microstructure of the alloy is illustrated at different magnification, which shows the presence of inclusions and subgrains. This is an expected results as the inclusions play a significant role in the stress-induced phase transformation mechanisms and, consequently, in the macroscopic pseudo-elastic response of the alloy.

a)   b)
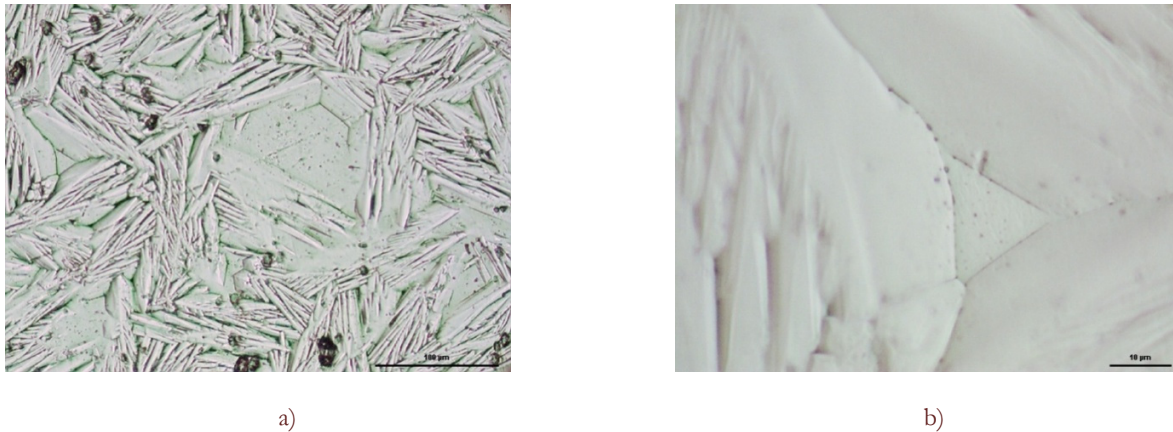
Figure 2: Initial austenitic microstructure of the investigated NiTi alloy: a) at low magnification showing the presence of inclusions, b) high magnification with presence of subgrains.

The engineering stress-strain curve of the material is illustrated in Fig 3, which were obtained from isothermal tensile tests, carried out at room temperature (T=298 K) by using a servo hydraulic universal testing machine, equipped with an electrical extensometer with a gauge length of 10 mm to measure the engineering deformations of standard dog-bone shaped specimen. In particular, Fig. 3.a shows the stress-strain curve obtained from a monotonic tensile test to fracture, while Fig. 3.b illustrates the marked hysteretic behavior of the material obtained from a loading-unloading cycle up to a maximum deformation of about 6.1 %. Furthermore, Fig. 3.b also illustrates the values of the main thermomechanical parameters of the alloys, *i.e.* the Young's moduli of austenite (E_A) and martensite (E_M), the transformation stresses from austenite to martensite (σ_s^{AM} and σ_f^{AM}), the stresses for reverse transformation from martensite to austenite (σ_s^{MA} and σ_f^{MA}), the uniaxial transformation strain (ε_L) and the Clausis-Clapeyron constant of the material ($C=d\sigma/dT$).

The evolution of the microstructure during uniaxial deformation was analyzed by a miniature testing machine which allows *in-situ* scanning electron microscopic (SEM) observations as well as X-Ray micro-diffraction analyses. In particular, the testing machine is equipped with a simple and removable loading frame, which allows SEM and X-Ray analyses at fixed values of applied load and/or deformations. The machine is powered by a stepping motor, which applies the mechanical deformation to the specimen through a calibrated screw, with pitch of 0.8mm, and a control electronic allows simultaneous measurement and/or control of applied load and stroke of the specimen head. The stroke is measured by a Linear Variable Differential Transformer (LVDT) while the load is measured by two miniaturized load cells with maximum capacity of 10 kN. Miniature dog bone shaped specimens with dimension showed in Fig. 4 were machined from NiTi sheets, by wire electro discharge machining, due to the poor workability of this class of materials by conventional machining processes as well as to reduce the formation of thermo-mechanical affected zone.

Step by step isothermal tensile tests were carried out, at room temperature, at increasing values of the specimen elongation. In particular, three levels of elongation have been applied, δ=0.8, 1.6 and 2.4 mm, which can be expressed as gross engineering strain (ε_g) with respect to the gauge length L_0=16 mm, *i.e.* ε_g=5, 10 and 15%. In particular, for each loading step the loading frame containing the specimen was removed from the testing machine, at fixed values of deformation, and analyzed by means of a Philips diffractometer in order to evaluate XRD spectra. XRD measurements were made with a Philips X-PERT diffractometer equipped with a vertical Bragg–Brentano powder goniometer.

A step–scan mode was used in the 2θ range from 30° to 90° with a step width of 0.02° and a counting time of 2 s per step. The employed radiation was monochromated CuKα (40 kV – 40 mA). The calculation of theoretical diffractograms and the generation of structure models were performed using the PowderCell software [20].

Furthermore, the gross engineering strain has been correlated to the effective engineering strain by a finite element simulation as reported in the following section.
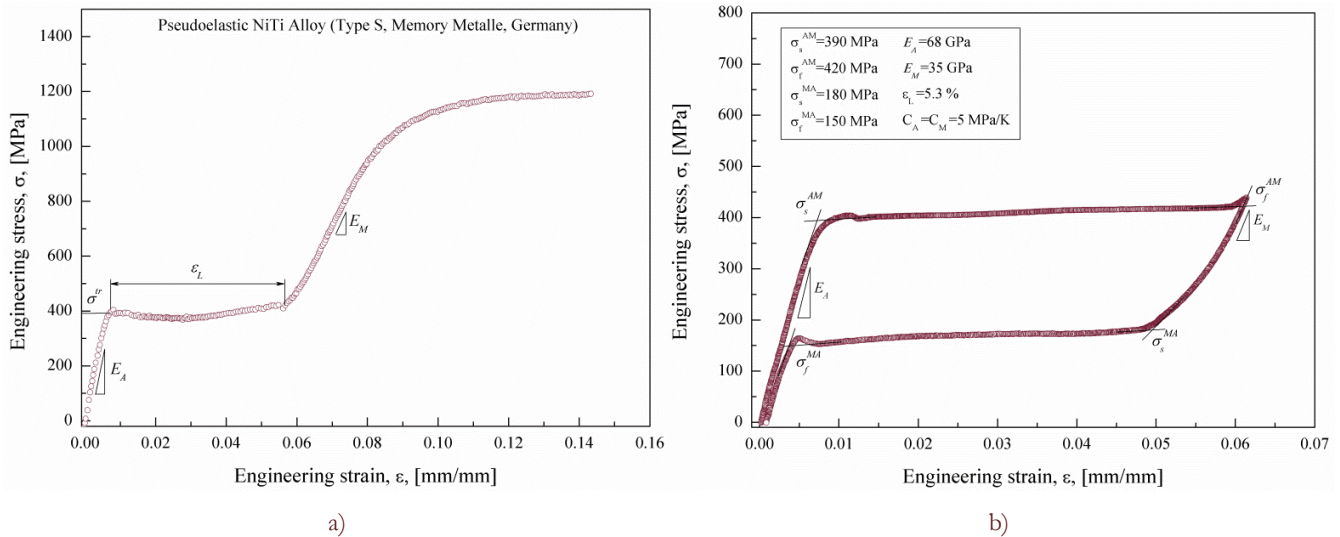

Figure 3: Isothermal stress-strain curve of the investigated alloy carried out at room temperature (T=298k): a) monotonic loading to fracture and b) loading-unloading cycle.
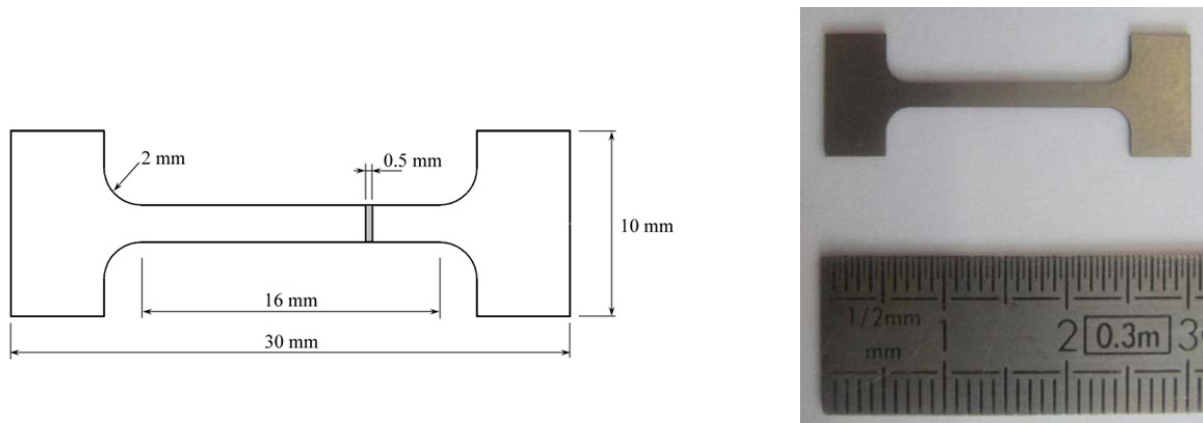

Figure 4: Uniaxial miniaturized specimens.

RESULTS AND DISCUSSION

Finite Element Analyses (FEA) were carried out in order to correlate the gross engineering strain (ε_g) to the effective engineering strain (ε_e), *i.e.* to the experimentally measured engineering stress-strain curve of Fig. 3. To this aim a 2D FE model was made, by using a commercial software, to simulate the testing conditions of the miniature specimen, and a standard non-linear solutions were adopted to model the complex stress strain behavior of the material illustrated in Fig 3. In particular, a quarter of the miniature specimen was modeled, due to symmetric geometry and boundary conditions, together with a part of the loading frame, and contact conditions were defined between them in order to reproduce the testing conditions as close as possible to reality. Fig. 5.a illustrates the FE mesh which consists of about 800 4-noded plane stress quadrilateral elements while Fig. 5.b shows the equivalent stress fringes corresponding to the maximum elongation of the specimen during cyclic tests (δ=2.4 mm and ε_g=15%).

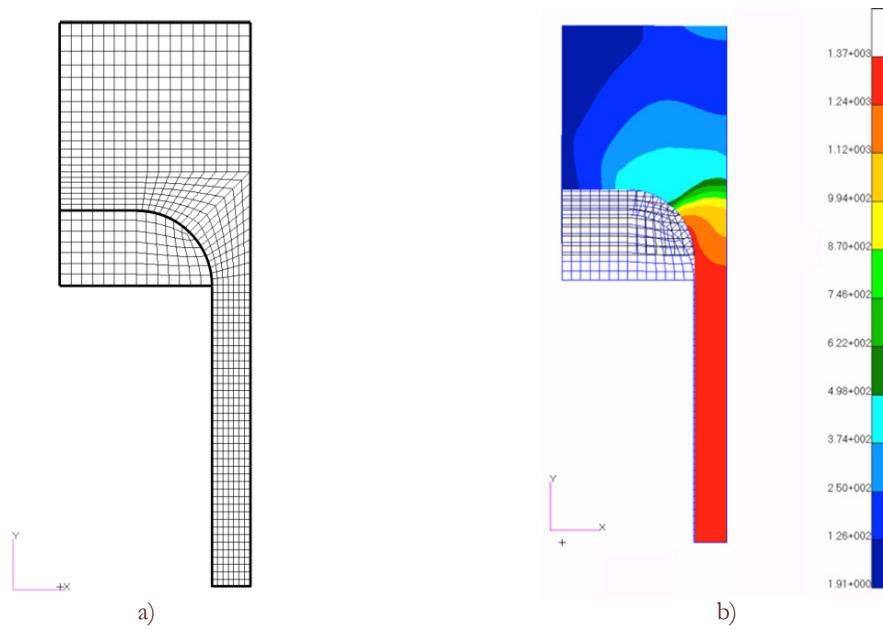a)   b)

Figure 5: FE analysis of the testing condition: a) FE model and b) equivalent stress fringes at the maximum elongation.

In Fig. 6a a comparison between the experimentally measured engineering stress-strain curve of Fig. 3 and the numerically simulated one is illustrated, and a good agreement is observed.

Fig. 7 shows a comparison between the numerically simulated stress-strain curve relative to net and gross engineering strain. This latter was calculated from the displacement of the specimen head, according to the experimental conditions.

As expected, gross strain is significantly greater than net strain and the difference increases when increasing the applied stress. Furthermore, this effect is also evident in the early stage of loading, *i.e.* in the range of elastic deformation of austenite, resulting in an apparent smaller value of the Young's modulus. This effect can be attributed to two different mechanisms: the compliance of the miniaturized testing machine and the deformation on the specimen heads. Note that a linear correction of the gross strain cannot be used here as the material non-linearity causes a marked non-linear relation between gross and net strain. For a better understanding of the results reported in the following section, Fig. 7 illustrates the relation between gross strain and net strain within the range of deformation of the experiments.
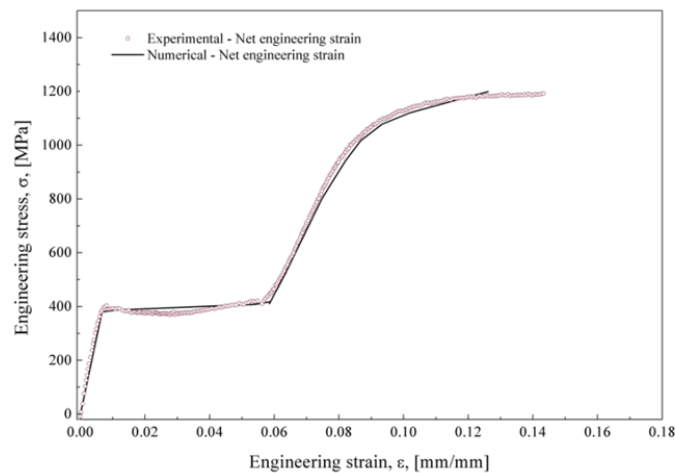

Figure 6: Comparison between experimentally measured stress-strain curve and numerically simulated one.

Prior to investigate stress strain behavior and in order to investigate microstructural transitions it is necessary to evaluate the initial XRD spectrum. The first diffraction obtained on the calibrated length of the miniature specimen in stress free conditions, shows two picks at 42.39 and 77.54°, corresponding to [011] and [022] crystallographic plains, typical of the

austenitic phases as illustrated in Fig. 2 at different magnifications. Using Bragg's low, the cell parameter evaluated for the two picks is about 3.012 Å.
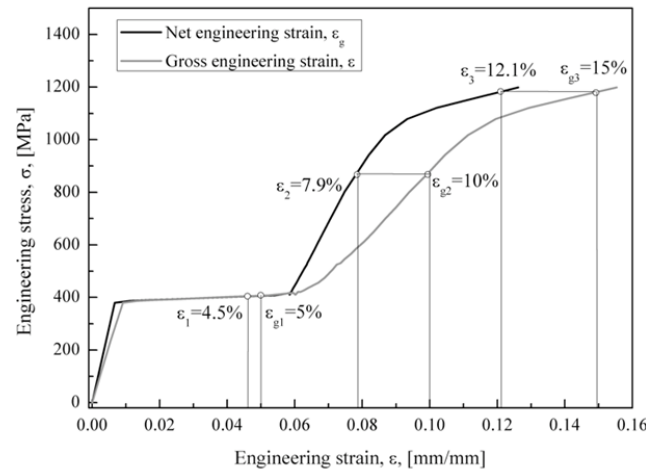
Figure 7: Relation between gross and net engineering strain obtained from FE simulations.
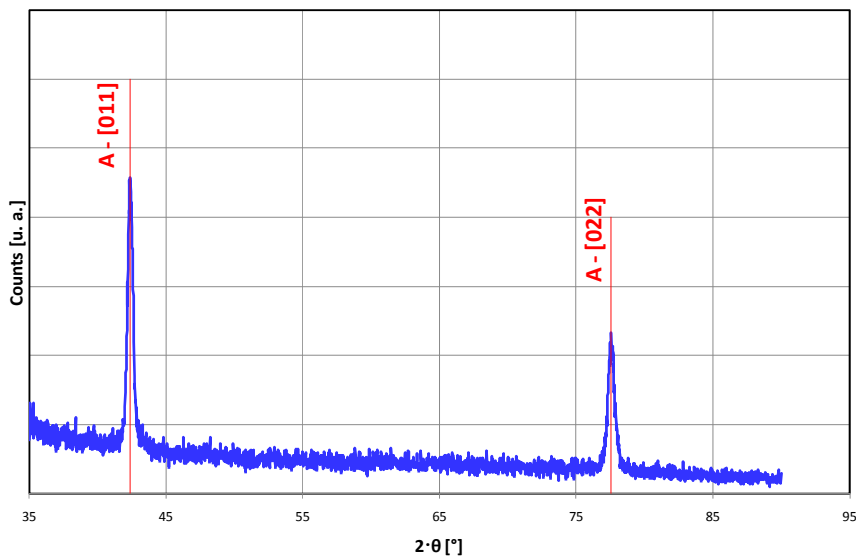
Figure 8: X-Ray spectra of the investigated NiTi alloy in stress free condition.

The evolution of the microstructure during mechanical loading and subsequent unloading was analyzed by XRD investigations carried out at fixed values of applied deformations. In particular, when loading up to the gross engineering strain ε_g=5%, corresponding to the effective engineering strain ε_e=4.5% and to a stress σ=400 MPa (Fig. 7), a different spectra was obtained with respect to the stress-free condition, as illustrated in Fig. 9; in fact three new pecks at different angles (42.99, 78.17 and 80.29°) are observed and, as expected, these new pecks reveal the presence of another phase which is obtained on stress plateau of the σ−ε curve. In addition, the simultaneous presence of two phases indicate an incomplete transformation, *i.e.* a partial transformation from austenite to a martensite, characterized by different cell parameter and different lattice.

Evidence of phase transition is confirmed when increasing the gross deformation to ε_g=10%, corresponding to the effective engineering strain ε_e=7.9% and to a stress of about σ=800 MPa (Fig. 7); this loading condition corresponds to the fully transformed martensitic structure as illustrated in Fig. 7. In this case the new phase is completely developed and his spectra is illustrated in Fig. 10, where five picks are observed corresponding to a monoclinic phase characterized by three cell parameters of about a=b=3.800 Å, c=2.600 Å and α=80°. The Miller indexes of the three peaks are:

- ✓ [120] for 43.55°;
- ✓ [112] for 54.39°;
- ✓ [030] for 59.90°;
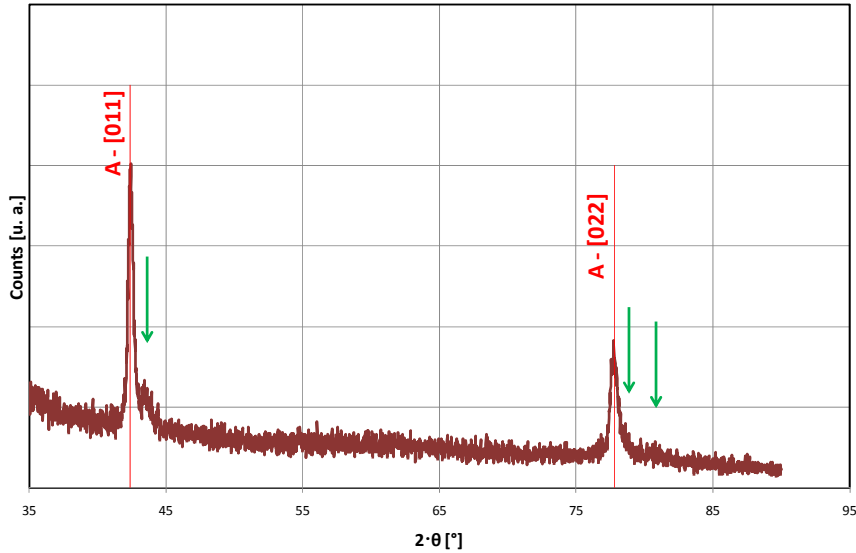- ✓ [003] for 78.72°;
- ✓ [113] for 80.80°.

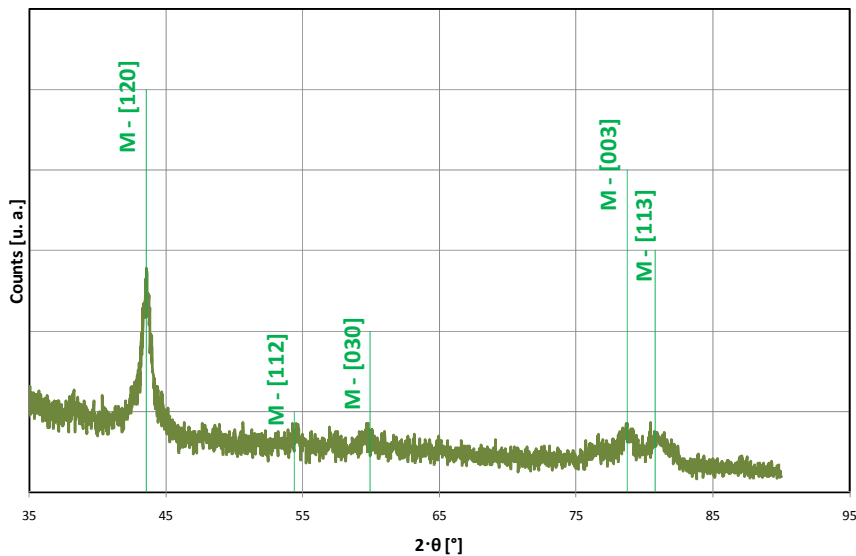Figure 9: X-Ray spectra obtained from monotonic loading up to ε_g=5%.

Figure 10: X-Ray spectra obtained from monotonic loading up to ε_g=10%.

When unloading from ε_g=10% to ε_g=5% martensite peaks [112] and [030] are not clearly evident, while [011] and [022] austenitic peaks grows which demonstrates the presence of both phases with a greater quantity of martensite as shown in Fig. 11. It is worth noting that the X-Ray spectra obtained during the monotonic loading stage under the same value of applied deformation is completely different, as shown in Fig. 9, where the main phase was the austenite. This is a direct consequence of the marked hysteretic behavior of the material, as shown in Fig. 3.b.

The final step of the mechanical cycle consists in complete unloading, *i.e.* the applied load is removed and a final diffraction test was carried out; the corresponding spectra was compared with the initial one, as illustrated in Fig. 12, in order to observe possible irreversible effects during loading unloading cycles. The figure shows good agreement between

the two spectra, which indicates a complete recovery of initial structure. In particular, no residual martensitic structure has been observed confirming a good pseudo-elastic behavior of the alloy. However, a coexistence of the two phases (austenite and martensite) is expected if further increasing the applied deformation, as a consequence of the formation of stabilized martensite, and this mechanisms will be analyzed in future investigations.
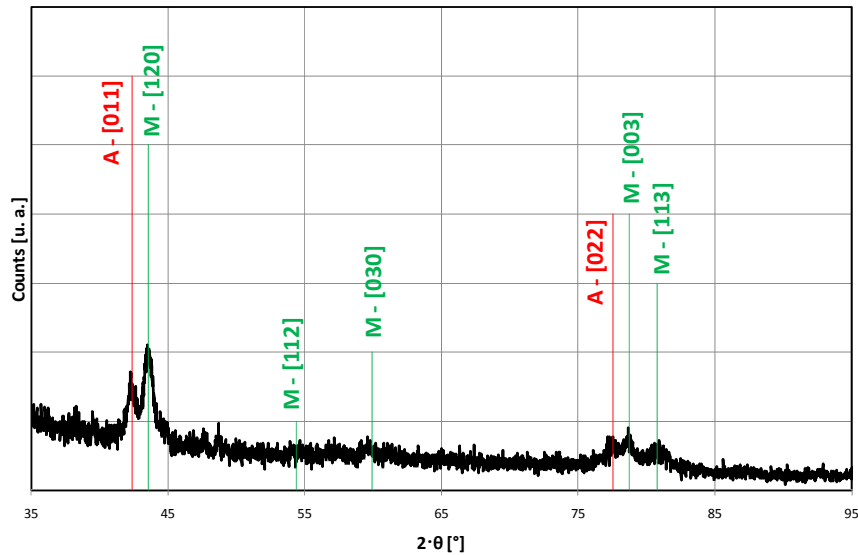
Figure 11: X-Ray spectra of obtained from unloading from ε_g=10% to ε_g=5%.
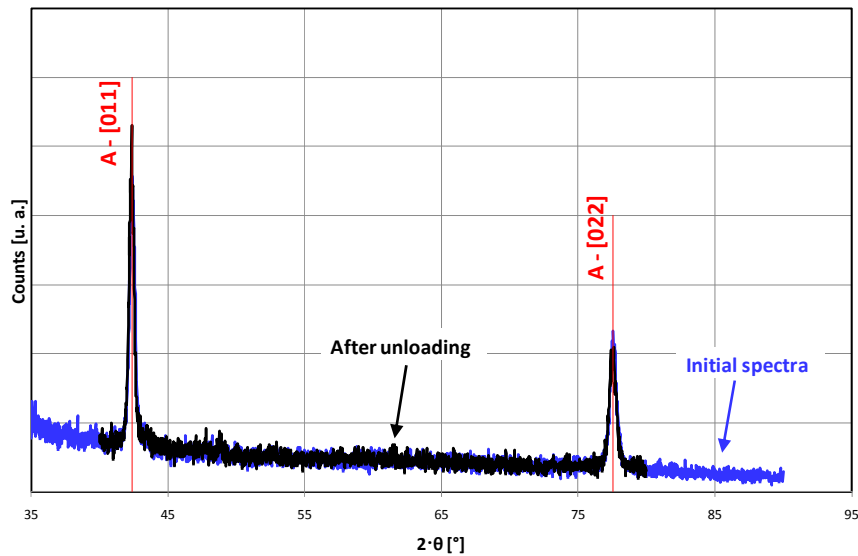
Figure 12: Comparison of the X-Ray spectra between initial condition and final stress free condition after unloading.

CONCLUSIONS

In this work a pseudo-elastic NiTi shape memory alloy has been investigated by using a miniaturize testing machine, which allows to analyze the microstructure evolution of the alloy at fixed values of applied load or deformations, by *in-situ* X-Ray analysis. In particular, miniaturized uniaxial specimens were used and the micro-structure evolution at increasing values of applied deformations was analyzed. The results can be summarized as follows:

✓ an initial cubic structure, with cell parameter of about 3.012 Å, characterizes the investigated alloy in stress free conditions;

✓ when loading up to an applied deformation ε_g=5%, corresponding to about σ=400 MPa in the stress plateau of the $\sigma-\varepsilon$ curve, a new phase, the martensitic one, is observed; as well known the stress plateau is attributed to the transition from initial cubic structure to the new structure;

✓ when increasing the deformation up to ε_g=10%, corresponding to about σ=800 MPa in the fully martensitic region of the $\sigma-\varepsilon$ curve, the new structure is completely developed and the initial structure is not observed. The new structure is characterized by monoclinic cells with three cell parameters of about a=b=3.800 Å, c=2.600 Å and α=80°;

✓ when unloading from ε_g=10% to ε_g=5% a different microstructure is observed with respect to the loading stage under the same value of applied deformation; this is a direct consequence of the marked hysteretic behavior of the material;

✓ after complete unloading the specimen recovers his initial shape and it shows the same diffraction spectra of the alloy in its initial condition; this indicate that the initial micro-structure is completely recovered without the formation of stabilized martensite.

REFERENCES

[1] K. Otsuka, X. Ren, Progress in Materials Science, (2005) 511.
[2] Y. Liu, G. S. Tan, Intermetallics, (2000) 8.
[3] V. Abbasi-Chianeh, J. Khalil-Allafi, Materials Science and Engineering A, 528, (2011), 5060-5065.
[4] X Yan, J Van Humbeeck, Journal of Alloys and Compounds, 509, (2011), 1001-1006.
[5] C.Urbina, S. De la flor, F.Ferrando, Materials Science and Engineering A, 501, (2009), 197-206.
[6] Y. Liu, D. Favier, Acta Mater, (2000) 48.
[7] K. C. Russel, Phase transformation, Ohio, ASM, (1969) 1219.
[8] S. Miyazaki, M. Kimura, H. Horikawa, In: Advance materials, K. Otsuka, Y. Fukai, editors. 93, V/B, Elsevier (1994) 1097.
[9] M. Pattabi, K. Ramakrishna, K.K. Mahesh, Materials Science and Engineering A, 448 (2007) 33.
[10] A. Sato, E. Chishima, K. Soma, T. Mori, Acta Metall, 30 (1982) 1177.
[11] K. Otsuka, K. Shimizu. Scripta Metall, 11 (1977) 757.
[12] G.V. Kurdjumov, L. G.Khandros, Dokl Nauk, SSSR, 66 (1949) 211.
[13] J. W., Christian, The theory of transformations in metals and alloys, Oxford: Pergamon Press, (1965) 815.
[14] K. Bhattacharya, S. Conti, G. Zanzotto, J. Zimmer. Nature, 428 (2004) 55.
[15] J. A. Krumhansl, G. R. Barsch, Proceedings of the International Conference on Martensitic Transformations '92, Ed. C. M. Wayman and J. Perkins (Monterey Institute of Advanced Studies, Carmel, 1993).
[16] A. Nagasawa, Y. Morii, Mater Trans JIM, 34 (1993) 855.
[17] A. Planes, Ll. Mañosa, Solid State Phys, 55 (2001) 159.
[18] K. Otsuka, X. Ren, Intermetallics, 7 (1999) 511.
[19] K. Otsuka, X. Ren, Mater Sci Eng A, 89 (1999) 273.
[20] PowderCell 2.3—Pulverdiffraktogramme aus Einkristalldaten und Anpassung experimenteller Beugungsaufnahmen. Available at http://www.bam.de/de/service/publikationen/powder_cell.htm.